DEUTSCHES ELEKTRONEN-SYNCHROTRON

DESY

DESY 96-162
August 1996

Studies of Diffractive Interactions Using the H1 Detector

P. R. Newman

School of Physics and Space Research, University of Birmingham, UK

S. Tapprogge

Institut für Hochenergiephysik, Universität Heidelberg

J. Theissen

III. Physikalisches Institut B, Physikzentrum, RWTH Aachen

A. Valkárová

Nuclear Center of Charles University, Prague, Czech Republic

S. Schiek, G. Schmidt

II. Institut für Experimentalphysik, Universität Hamburg

B. Clerbaux

Université Libre de Bruxelles, Belgium

ISSN 0418-9833

NOTKESTRASSE 85 - 22607 HAMBURG

To be sure that your preprints are promptly included in the
HIGH ENERGY PHYSICS INDEX,
send them to (if possible by air mail):

DESY **Bibliothek** **Notkestraße 85** **22607 Hamburg** **Germany**	**DESY-IfH** **Bibliothek** **Platanenallee 6** **15738 Zeuthen** **Germany**

DESY 96-162
August 1996

ISSN 0418-9833

STUDIES OF DIFFRACTIVE INTERACTIONS USING THE H1 DETECTOR

P.R. NEWMAN
School of Physics and Space Research, University of Birmingham B15 2TT, England.

S. TAPPROGGE
Institut für Hochenergiephysik, Universität Heidelberg Schröderstr. 90, D-69120 Heidelberg, Germany

J. THEISSEN
III. Physikalisches Institut B, Physikzentrum, RWTH Aachen D-52056 Aachen, Germany

A. VALKÁROVÁ
Nuclear Center of Charles University V. Holešovičkách 2, Prague, Czech Republic

S. SCHIEK, G. SCHMIDT
University of Hamburg, II. Institut für Experimentalphysik Notkestraße 85, D-22607 Hamburg, Germany

B. CLERBAUX
Université Libre de Bruxelles Bd du Triomphe, B-1050 Brussels, Belgium

H1 COLLABORATION.

Investigations of diffractive interactions using data taken in 1994 with the H1 detector at HERA are presented, in the form of the contributions to the International Workshop on Deep-Inelastic Scattering and Related Phenomena, Rome, April 1996. This report covers inclusive measurements of diffraction both in deep-inelastic scattering and in photoproduction, energy flow and open charm production in diffractive deep-inelastic scattering, jet studies at all Q^2, a thrust analysis of diffractive deep-inelastic scattering and photoproduction and electroproduction of vector mesons.

INCLUSIVE MEASUREMENTS OF DIFFRACTION IN DEEP-INELASTIC SCATTERING AND PHOTOPRODUCTION [a]

P.R. NEWMAN
School of Physics and Space Research, University of Birmingham, B15 2TT, England.

A precision measurement of diffractive deep-inelastic ep scattering is presented in the form of the structure function, $F_2^{D(3)}(\beta, Q^2, x_{I\!P})$. Factorisation of the $x_{I\!P}$ dependence is found to be broken. The Q^2 and β dependences are examined after averaging $F_2^{D(3)}$ over $x_{I\!P}$. Unambiguous violations of scale invariance are observed. Perturbative QCD fits based on DGLAP evolution favour a "leading" gluon distribution carrying in excess of 80% of the momentum of the exchange. Also presented is the differential cross-section, $d\sigma^D/dM_X^2$ for diffractive photoproduction processes in which the proton remains intact and a system of mass M_X is produced at the photon vertex. It displays a quasi-elastic peak and a higher mass continuum, both of which are consistent with Regge predictions based on a soft pomeron.

1 Introduction

Following the observation at HERA in 1992 of deep-inelastic scattering (DIS) events with a large region of rapidity around the proton remnant direction devoid of hadron production,[1,2] data taken in 1993 were used to quantify the contribution of such events to the DIS cross-section, by the measurement of a structure function $F_2^{D(3)}$.[3,4] This demonstrated that the rapidity gap events could dominantly be attributed to diffraction and gave the first indications of a large gluonic contribution to the partonic sub–structure of the exchange.[5,6] Considerably more precise 1994 preliminary H1 results on the diffractive structure function in an extended kinematic range are presented here.

Results from HERA on the total γp cross-section,[7,8] and exclusive light vector meson photoproduction [9,10] have been well described in the Regge picture in terms of a single pomeron trajectory, consistent with that obtained by Donnachie and Landshoff in fits to pp and $\bar{p}p$ total cross-sections.[11] The first inclusive measurements of the invariant mass distribution of the products of diffraction dissociation of real photons at HERA energies are also presented here.

[a] First presented at the Topical Conference on Hard Diffraction, Eilat, Israel, February 1996.

2 Diffractive Deep-Inelastic Scattering

2.1 Experimental Method

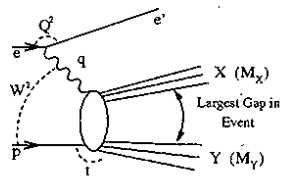

Figure 1: Schematic illustration of the method of decomposing events to define diffractive cross-sections, showing the kinematic variables discussed in the text.

The measured cross-section is defined in terms of the generalised process, $ep \rightarrow e'XY$, illustrated in figure 1. The hadronic final state in any event may be decomposed into two systems, X and Y, that are separated by the largest gap in the rapidity distribution of hadrons in the $\gamma^* p$ centre of momentum frame. A cross-section is then measured at different values of the masses, M_X and M_Y, of the two systems. When both masses are small by comparison with the centre of mass energy, a large rapidity gap must always occur from kinematic considerations alone, and the t-channel diffractive exchange dominates the process, $\gamma^* p \rightarrow XY$.

With q and P denoting 4-vectors for the virtual photon and the proton respectively and with X and Y denoting 4-vectors for the two distinct components of the hadronic final state, we define the standard kinematic variables

$$Q^2 = -q^2 \quad W^2 = (q+P)^2 \quad t = (P-Y)^2 \quad x_{I\!P} = \frac{Q^2+X^2}{Q^2+W^2} \quad \beta = \frac{Q^2}{Q^2+X^2}$$

The experimental selection of events is based on the presence of a rapidity gap spanning at least the laboratory range $3.0 < \eta < 7.5$, inferred from the absence of activity in the forward[b] components of the H1 detector.[12] The event kinematics are obtained by reconstructing M_X using all particles produced backward of the gap and from the measurement of a scattered electron in the Backward Electromagnetic Calorimeter.[12] The lower limit of 7.5 on the rapidity reached by particles in the leading baryonic system Y restricts its mass to $M_Y \lesssim 1.6$ GeV and implies that $|t| \lesssim 1.0$ GeV^2. This system is not directly observed, though by requiring $x_{I\!P} < 0.05$, we ensure that Y carries in excess of 95% of the incident proton momentum. Any isospin-exchanging process is strongly suppressed in this kinematic region. The contribution to the

[b]The forward direction is defined to be that of the outgoing proton beam, and corresponds to positive rapidities.

measured cross-section from events in which the proton dissociates is estimated to be at the level of 5% using the DIFFVM [14] Monte Carlo.

The data presented here correspond to an integrated luminosity of 2.0 pb^{-1}: a ten-fold increase in statistics compared to our earlier measurement.[3] A further 0.06 pb^{-1} of data taken with the interaction point shifted by 70 cm in the forward (proton) direction enable measurements to be made at lower values of Q^2 than has previously be possible.

2.2 The Diffractive Structure Function, $F_2^{D(3)}(\beta, Q^2, x_{I\!P})$

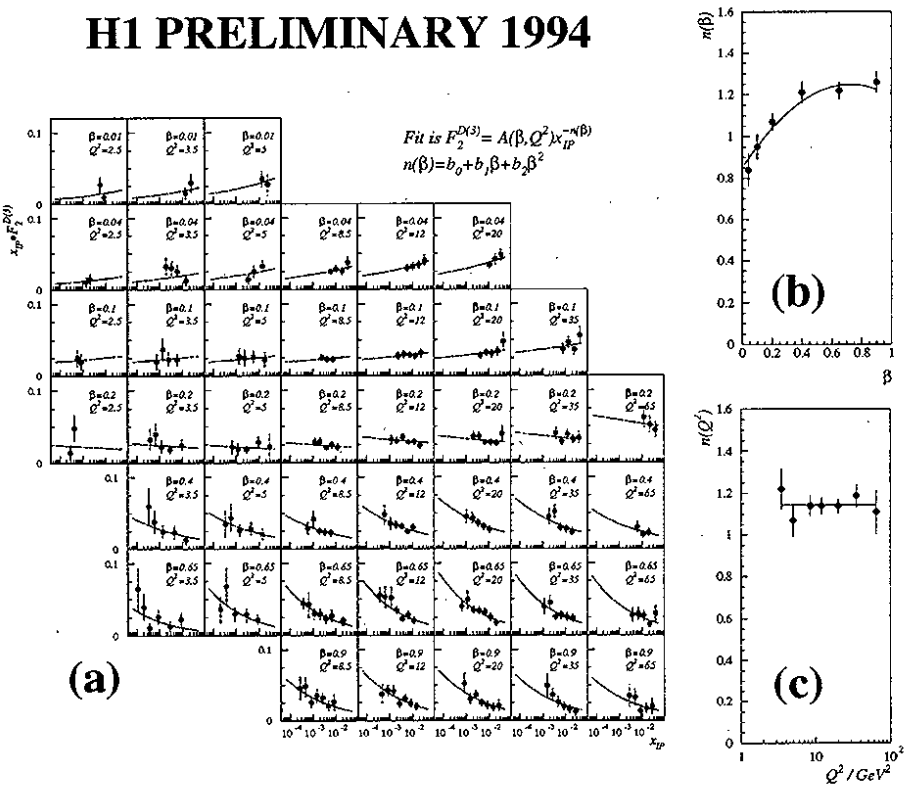

Figure 2: (a) $x_{I\!P} \cdot F_2^{D(3)}(\beta, Q^2, x_{I\!P})$ integrated over the range $M_Y < 1.6$ GeV and $|t| < 1$ GeV^2. (b) The β dependence of n when $F_2^{D(3)}$ is fitted to the form $F_2^{D(3)} = A(\beta, Q^2)/{x_{I\!P}}^{n(\beta)}$. (c) The Q^2 dependence of n when $F_2^{D(3)}$ is fitted to the form $F_2^{D(3)} = A(\beta, Q^2)/{x_{I\!P}}^{n(Q^2)}$. The experimental errors are statistical and systematic added in quadrature. The overall fit described in the text is shown in all three plots.

Following the proposal of Ingelman and Schlein,[13] the results are presented in terms of a diffractive structure function, $F_2^{D(3)}(\beta, Q^2, x_{I\!P})$, which is related to the differential $ep \to e'XY$ cross section by

$$\frac{\mathrm{d}^3\sigma^D_{ep\to eXY}}{\mathrm{d}x_{I\!P}\,\mathrm{d}\beta\,\mathrm{d}Q^2} = \frac{4\pi\alpha^2}{\beta Q^4}(1 - y + \frac{y^2}{2})F_2^{D(3)}(\beta, Q^2, x_{I\!P}). \quad (1)$$

The quantity, $x_{I\!P} \cdot F_2^{D(3)}(\beta, Q^2, x_{I\!P})$ is shown as a function of $x_{I\!P}$ in figure 2a, in the kinematic range $2.5 < Q^2 < 65$ GeV^2, $0.01 < \beta < 0.9$ and $0.0001 < x_{I\!P} < 0.05$. In a Regge interpretation[15] in which the $x_{I\!P}$ dependence describes a pomeron flux associated with the proton, one expects a behaviour of the form, $F_2^{D(3)} \propto \frac{1}{x_{I\!P}^n}$, with $n \simeq 2\alpha(0) - 1$, where $\alpha(t) = \alpha(0) + \alpha' t$ is the pomeron trajectory [c]. Figure 2b shows the results of a fit to this form when n is allowed to vary with β but not with Q^2. The improved precision and enhanced kinematic range reveal deviations from the universal factorisation previously reported,[3] with n decreasing significantly with β for $\beta \lesssim 0.3$. The value of n at $\beta \gtrsim 0.3$ is slightly larger than that expected for a soft pomeron.[11] There are a number of potential explanations for the decrease in n for $\beta \lesssim 0.2$ to values below unity. One possibility is that there is a contribution from the exchange of meson trajectories (f, a_2 etc.), which have lower intercepts and softer β dependences than the leading vacuum trajectory. In a partonic interpretation of the diffractive exchange (see section 2.3), such an effect may occur if the β or $x_{I\!P}$ dependence differs for sea quark and gluon components of the exchange.[16]

In figure 2c, n is allowed to vary with Q^2 but not β. There is no evidence for any dependence of n on $\ln Q^2$. A purely illustrative, though acceptable fit in which the value of n varies quadratically with β and has no Q^2 dependence is superimposed in figures 2a–c.

2.3 The Partonic Structure of Diffractive Exchange

Integrating $F_2^{D(3)}$ over a fixed range in $x_{I\!P}$ yields a quantity which is proportional to the average structure function of whatever colourless exchanges contribute to the measured cross-section in the kinematic range accessed. We define

$$\tilde{F}_2^D(\beta, Q^2) = \int_{x_{I\!P}=0.0003}^{x_{I\!P}=0.05} F_2^{D(3)}(\beta, Q^2, x_{I\!P})\mathrm{d}x_{I\!P} \quad (2)$$

[c] In practice, the finite values of t at which the measurement takes place reduce n relative to $2\alpha(0) - 1$ by a few percent.

Where no measurement has been made, the fit shown in figure 2 is used to make extrapolations.

Fig. 3a shows $\tilde{F}_2^D(\beta, Q^2)$ as a function of Q^2 for fixed β and fig. 3b shows it as a function of β for fixed Q^2. No fast variation with Q^2 is observed, though violations of scaling are clearly established. A rise with $\ln Q^2$ persists to values of β far in excess of the point ($x \sim 0.15$) at which the structure of the nucleon is dominated by valence quarks rather than by gluons and $\frac{\partial F_2(x,Q^2)}{\partial \ln Q^2}$ correspondingly becomes negative.[17] The scaling violations of $\tilde{F}_2^D(\beta, Q^2)$ are thus in qualitative accord with the hypothesis of a substantial hard gluon component in the structure of the diffractive exchange. At fixed Q^2, $\tilde{F}_2^D(\beta, Q^2)$ displays little dependence on β. There is no evidence for the fall with increasing parton momentum fraction characteristic of hadron structure functions. A

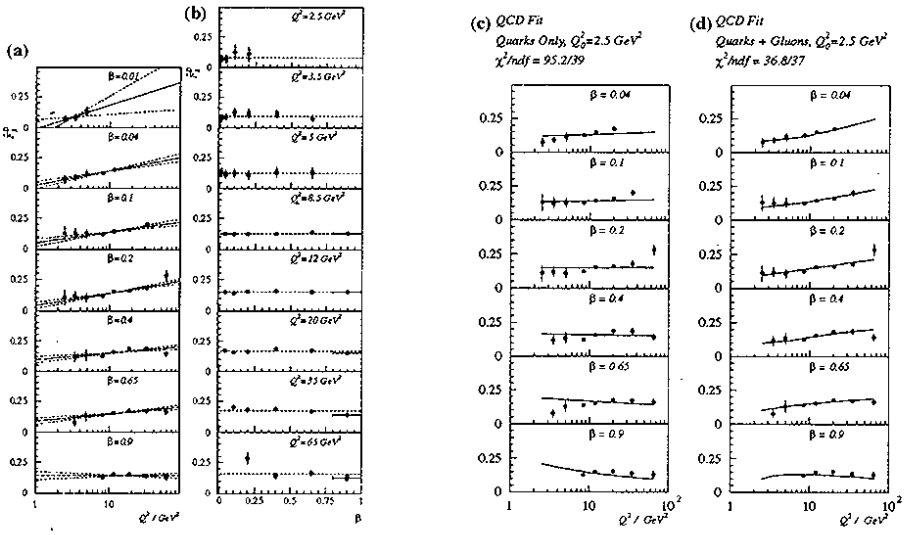

Figure 3: (a) $\tilde{F}_2^D(\beta, Q^2)$ as a function of Q^2 for different β values. The superimposed lines correspond to the best fit to a linear dependence on $\ln Q^2$ (continuous) and $\pm 1\sigma$ (dashed). (b) $\tilde{F}_2^D(\beta, Q^2)$ as a function of β for different Q^2 values, with a best fit to a constant β dependence. c) DGLAP QCD comparison of the (β, Q^2) dependence of $\tilde{F}_2^D$ assuming only quarks at the starting scale of $Q_0^2 = 2.5\,\mathrm{GeV}^2$; d) DGLAP QCD comparison of the (β, Q^2) dependence of $\tilde{F}_2^D$ assuming both quarks and gluons at the starting scale.

QCD analysis of $\tilde{F}_2^D(\beta, Q^2)$ confirms this qualitative picture.[5,6,18] A u+d+s flavour singlet quark and a gluon distribution are parameterised at a starting

scale, $Q_0^2 = 2.5$ GeV^2, as

$$x_{i/\mathbb{P}} \cdot f_i(x_{i/\mathbb{P}}) = A_i \, x_{i/\mathbb{P}}^{B_i} \, (1 - x_{i/\mathbb{P}})^{C_i} \tag{3}$$

where $i = q, g$ and $x_{i/\mathbb{P}}$ is the fraction of the exchange momentum carried by the parton. These parton distributions are evolved using DGLAP [19] evolution to $Q^2 > Q_0^2$, with the values of $A_{q,g}$, $B_{q,g}$ and $C_{q,g}$ as fit parameters [d]. Charm quarks are not explicitly introduced into the parton distributions, but are included through boson-gluon fusion using the procedure followed in [21].

Figure 3c shows the best fit obtained for $\tilde{F}_2^D$ when A_g is constrained to be zero, and only quarks contribute at the starting scale. Because of the persistence of rising $\ln Q^2$ scaling violations to high values of β, no such parameterisation is acceptable. An excellent fit, shown in figure 3d, can be obtained when gluons are also introduced at the starting scale.

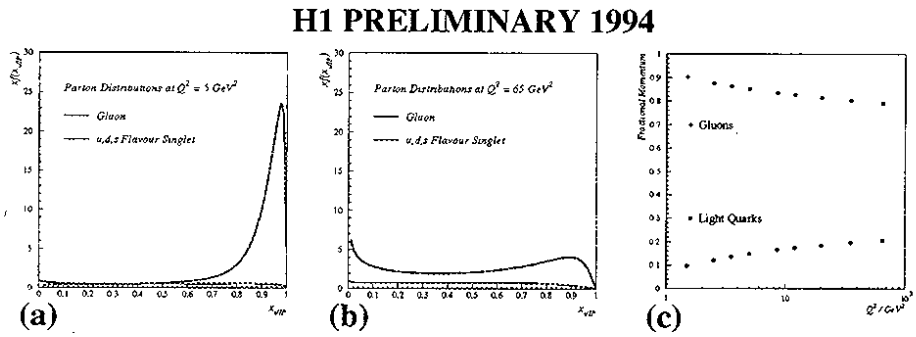

Figure 4: Quark and gluon momentum weighted distributions in fractional momenta $x_{g/\mathbb{P}}$ and $x_{q/\mathbb{P}}$ for diffractive exchange averaged over $x_{\mathbb{P}}$ and t extracted using the DGLAP QCD fit at (a) $Q^2 = 5$ GeV^2 and (b) $Q^2 = 65$ GeV^2; c) fraction of the total momentum transfer carried by quarks and by gluons at each Q^2; no errors are shown in the plots because of ambiguity in their determination due to the tendency of the solution to peak at large $x_{g/\mathbb{P}}$.

The parton densities in the mixed quark and gluon fit at $Q^2 = 5$ GeV^2 and $Q^2 = 65$ GeV^2 are shown in figure 4, along with the integrated momentum fractions carried by quarks and gluons as a function of Q^2. At $Q^2 = 5$ GeV^2, a "leading" gluon behaviour is observed, in which the exchange is dominated by gluons carrying fractional momentum, $x_{g/\mathbb{P}} > 0.9$, tending to a singularity as $x_{g/\mathbb{P}} \to 1$. As Q^2 increases, the gluon distribution in the solution evolves in the usual way to lower values of β. Throughout the Q^2 range, in excess

[d] Since additional theoretical input is required to normalise the structure function, and since it is far from clear that one should exist for space-like exchanges [20], no momentum sum rule is imposed.

of 80% of the exchange momentum is carried by gluons. H1 analyses of the hadronic final state in diffractive DIS lend support to these conclusions[22]. The "leading" gluon behaviour is expected in models of deep-inelastic diffraction such as that proposed by Buchmüller and Hebecker.[23]

3 Diffraction in Photoproduction

Similar techniques [24] to those employed in the DIS case have been used to measure inclusive cross-sections for diffractive photoproduction at a γp centre of mass energy averaged over the photon flux of $\langle W \rangle = 187$ GeV. Figure 5

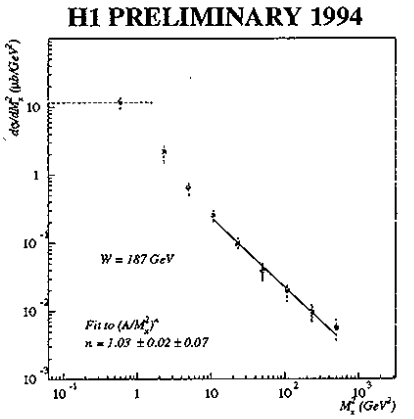

Figure 5: Corrected points obtained for the t-integrated cross-section, $d\sigma^D/dM_X^2\,(\gamma p \to Xp)$ at $Q^2 = 0$ and $\langle W \rangle = 187$ GeV. A fit to the form, $(1/M_X^2)^n$ is shown for $10.8 < M_X^2 < 500$ GeV^2.

shows the t-integrated cross-section, $d\sigma^D/dM_X^2$ for photoproduction processes that are elastic at the proton vertex[e]. In the "triple Regge" region ($M_X^2 \to \infty$, $W^2/M_X^2 \to \infty$), the dynamics of dissociation processes have been shown [25] to be well described by combinations of triple Regge amplitudes, which at low values of M_X^2/W^2 are dominated by the triple pomeron amplitude.[26] Assuming that the triple pomeron diagram dominates and parameterising the product of the triple pomeron coupling and the couplings of the pomeron to external particles[f] by $e^{b_0 t}$, the differential cross-section is expected to behave at fixed W as [15]

[e] A correction at the level of 5% is made to remove proton dissociative events.

[f] In the measured region, the minimum kinematically permissible value of $|t|$ is close to zero.

$$\frac{d\sigma^D}{dM_X^2} \sim \left(\frac{1}{M_X^2}\right)^{\alpha(0)} \cdot \left(b_0 + 2\alpha' \ln \frac{W^2}{M_X^2}\right)^{-1} \tag{4}$$

For $10.8 < M_X^2 < 500$ GeV^2, a fit to the form, $\frac{d\sigma^D}{dM_X^2} \sim (1/M_X^2)^n$ is shown in figure 5. The result of the fit is $n = 1.03 \pm 0.02$(stat.) $\pm$ 0.07(syst.), illustrating that the data display the approximate $1/M_X^2$ dependence characteristic of diffractive dissociation. A fit to the full form of equation 4 yields $\alpha(0) = 1.11 \pm 0.02$(stat.) $\pm$ 0.07(syst.), where we have taken $\alpha' = 0.25$ GeV^{-2} and $b_0 = 3 \pm 1$ GeV^{-2}, estimated from fixed target data.[27] This result confirms that the dominant contribution to the cross-section for the dissociation of photons to low mass states arises from the triple pomeron amplitude. The proximity of the extracted $\alpha(0)$ to the established value of 1.08 [11] also provides a control for the measurement of F_2^D.

Monte Carlo models are used to unfold the points in figure 5 to separate total cross-sections for quasi-elastic and dissociative diffractive photoproduction processes. We obtain $\sigma(\gamma p \rightarrow Vp) = 18.2 \pm 0.8$(stat.) $\pm$ 2.8(syst.) μb, where $V = \rho^0$, ω or ϕ, and $\sigma(\gamma p \rightarrow Xp) = 21.5 \pm 0.6$(stat.) $\pm$ 5.9(syst.) μb where X is any other state with $M_X^2/W^2 < 0.05$. These measurements confirm our previous results [7] and uncertainties are reduced.

4 Summary and Conclusions

Diffractive deep-inelastic ep scattering at HERA has been investigated using the data taken in 1994 with the H1 detector. At the present level of experimental precision, the dependence on $x_{I\!P}$ of the diffractive structure function, $F_2^{D(3)}(\beta, Q^2, x_{I\!P})$, is found to vary with β but not with Q^2. The scaling violations in the Q^2 dependence of $\tilde{F}_2^D(\beta, Q^2)$ for fixed β are shown to be interpretable in the framework of QCD in terms of parton densities that are dominated by a gluon distribution that peaks strongly as $x_{g/I\!P} \rightarrow 1$ and carries approximately 80% of the momentum of the diffractive exchange.

A measurement of the invariant mass distribution of the component of the final state produced at the photon vertex in diffractive photoproduction processes where the proton remains intact shows a peak in the region of the light vector mesons, ρ, ω and ϕ and a dissociation continuum at larger masses. In the triple Regge region, the cross-section is in good agreement with a prediction based on the triple pomeron amplitude.

Acknowledgements

We are grateful to the HERA machine group and to H1's engineers and technicians for their work in constructing and now maintaining the HERA accelerator and the H1 detector. We thank our funding agencies for financial support, the DESY technical staff for continual assistance; and the DESY directorate for the hospitality which they extend to the non–DESY members of the collaboration. The author wishes to acknowledge the help of many members of the H1 collaboration with the preparation of this contribution.

References

1. ZEUS Collaboration, M. Derrick et al., Phys. Lett. **B315** (1993) 481.
2. H1 Collaboration, T. Ahmed et al., Nucl. Phys. **B429** (1994) 477.
3. H1 Collaboration, T. Ahmed et al., Phys. Lett. **B348** (1995) 681.
4. ZEUS Collaboration, M. Derrick et al., Z. Phys **C68** (1995) 569.
5. J. Phillips, "Rapidity Gap Events at HERA and the Structure of the Pomeron", in Proc. of the International Workshop on Deep–Inelastic Scattering and Related Topics, Paris, France, April 1995, p.359.
6. J. Dainton, "Deep–Inelastic Electron-Proton Diffraction", DESY **95-228**.
7. H1 Collaboration, S. Aid et al., , Z. Phys **C69** (1995) 27.
8. ZEUS Collaboration, M. Derrick et al., , Z. Phys **C63** (1994) 391.
9. H1 Collaboration, S. Aid et al., Nucl. Phys. **B463** (1996) 3.
10. ZEUS Collaboration, M. Derrick et al., Z.Phys. **C69** (1995) 39.
11. A. Donnachie, P. Landshoff, Phys. Lett. **B296** (1992) 227.
12. H1 Collaboration, I. Abt et al., "The H1 Detector at HERA", DESY **93–103**.
13. G. Ingelman and P. Schlein, Phys. Lett. **B152** (1985) 256.
14. B. List, Diploma Thesis, Techn. Univ. Berlin, unpublished (1993).
15. See for example P. Collins, "An Introduction to Regge Theory & High Energy Physics", Cambridge University Press, Cambridge (1977).
16. N. Nikolaev and B. Zakharov, Z. Phys. **C53** (1992) 331.
17. NMC Collaboration, M. Arneodo et al., Phys. Lett. **B364** (1995) 107;
    BCDMS Collaboration, A. Benevuti et al., Phys. Lett. **B223** (1989) 485.
18. C. Pascaud, F. Zomer, LAL preprint LAL/94-42.
19. Yu. Dokshitzer, JETP **46** (1977) 641.
    V. Gribov and L. Lipatov, Sov. Journ. Nucl. Phys. **15** (1972) 78.
    G. Altarelli and G. Parisi, Nucl. Phys. **B126** (1977) 298.
20. L. Trentadue and G. Veneziano, Phys. Lett. **B323** (1994) 201.
21. H1 Collaboration, T. Ahmed et al., "A Measurement and QCD Analysis of the Proton Structure Function $F_2(x, Q^2)$ at HERA", DESY **96-039**.
22. S. Tapprogge, J. Theissen, A. Valkarova, this report.
23. W. Buchmüller and A. Hebecker, Phys. Lett. **B355** (1995) 573.
24. P. Newman, "A Study of the Dynamics of Diffractive Photoproduction at HERA", PhD Thesis, University of Birmingham (February 1996), RAL-TH-96-011.
25. For a review, see K. Goulianos, Phys. Rep. **101** (1983) 169.
26. D. Roy and R. Roberts, Nucl. Phys. **B77** (1974) 240.
27. T. Chapin et al., Phys. Rev. **D31** (1985) 17.

ENERGY FLOW AND OPEN CHARM PRODUCTION IN DIFFRACTIVE DEEP-INELASTIC SCATTERING

S. TAPPROGGE

Institut für Hochenergiephysik, Universität Heidelberg
Schröderstr. 90
D 69120 Heidelberg, Germany

Measurements of the energy flow and of D^* meson production in diffractive deep-inelastic ep scattering at HERA are presented using data taken in 1994 with the H1 detector. Parton densities dominated by gluons, as obtained from a DGLAP QCD analysis of the diffractive structure function $F_2^{D(3)}(\beta, Q^2, x_{I\!P})$, are used together with a model of deep-inelastic electron pomeron scattering to make predictions for these processes. These predictions are found to be consistent with the present measurements.

1 Introduction

The analysis of the data taken by H1 in 1994 has provided a precise measurement [1] of the diffractive structure function $F_2^{D(3)}(\beta, Q^2, x_{I\!P})$ over an extended kinematical range. In the framework of the DGLAP QCD evolution equations, parton densities are obtained, according to which more than 80% of the momentum in the diffractive exchange is found to be carried by gluons [a]. The gluons exhibit a "leading" behaviour in the distribution of the fractional momentum.

In this contribution new H1 results on the hadronic final state (system X) in the process $ep \to e'XY$ are presented, where the systems X and Y are separated by the largest gap in rapidity, $M_Y < 1.6$ GeV/c^2 and $x_{I\!P} = (Q^2 + M_X^2)/(Q^2 + W^2) < 0.05$. These are the measurements of energy flow and open charm production, which provide sensitivity to the gluonic contribution in the diffractive exchange. They are compared to predictions obtained from the RAPGAP model [2], in which deep-inelastic diffraction is understood in terms of deep-inelastic electron-pomeron ($e I\!P$) scattering [3]. The parton densities used for the simulations are those obtained from the DGLAP QCD analysis [1] of the diffractive structure function $F_2^{D(3)}$.

[a] This observation can be related (within DGLAP) to the observed scaling violations of $F_2^{D(3)}$. For fixed β, $F_2^{D(3)}$ has been found [1] to increase with increasing $\log Q^2$, with the rise persisting up to high values of β.

2 Energy Flow in the $\gamma^* I\!P$ Centre-of-Mass System

In the $\gamma^* I\!P$ centre-of-mass system (which is the rest-frame of system X) the measured energy flow allows direct studies of the final state, avoiding effects of the boost to the laboratory frame. For the central region ($\eta^* \approx 0$) of this system more energy is expected to be produced for a gluon initiated process than for a quark initiated process. In the latter case, the produced two partons are mainly aligned with the $\gamma^* I\!P$ axis, whereas for a gluon initiated process less alignment of the partons is expected.

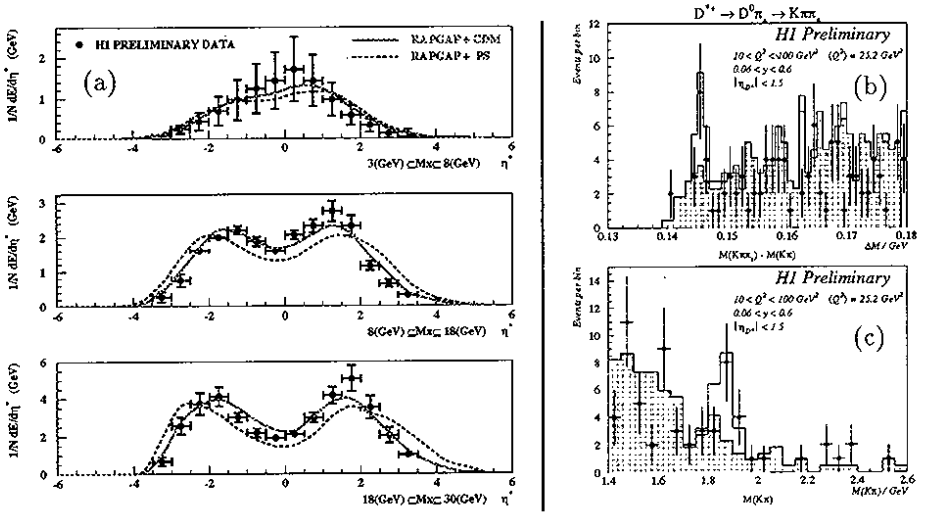

Figure 1: a) Energy flow in the $\gamma^* I\!P$ CMS – corrected for detector biases – compared to the predictions of the RAPGAP model using parton densities obtained from a DGLAP QCD analysis of the diffractive structure function $F_2^{D(3)}$; shown are two different approaches to the modelling of QCD cascades (CDM = Colour Dipole Model, PS = Parton Shower). Errors shown are statistical and systematic errors added in quadrature. b) mass difference between $K\pi\pi_{slow}$ and $K\pi$, requiring $|M_{K\pi} - M_{D^0}| < 80$ MeV/c^2. c) mass of the $K\pi$ system, requiring $|(M_{K\pi\pi_{slow}} - M_{K\pi}) - 145.4\ \text{MeV}/c^2| < 1.5$ MeV/c^2. For b) and c) the histogram is the prediction of the RAPGAP model using the parton densities obtained from the QCD analysis, the shaded histogram shows the RAPGAP events without a D^* meson

Fig. 1a) shows the measured energy flow (corrected for detector biases) in three bins of M_X compared to the prediction of the RAPGAP model using the parton densities as described above. The data are well described for two different approaches to the modelling of the QCD cascade in the final state (PS = Parton Shower in the "leading log" approximation[4], CDM = Color Dipole Model[5]). Not shown is the prediction of the RAPGAP model with unphysical

parton densities (only quarks, no gluons at all), which gives significantly less energy flow in the central region $\eta^* \approx 0$ than in the data.

3 Open Charm Production in Diffractive DIS

For a dominant gluon component in the diffractive exchange, the production of charm quarks via the boson–gluon fusion process is expected. $D^{*\pm}$ meson production has been searched for in the diffractive data by looking for the decay $D^{*\pm} \rightarrow D^0(\bar{D}^0)\pi^{\pm}_{slow} \rightarrow K^{\mp}\pi^{\pm}\pi^{\pm}_{slow}$. A signal for D^* mesons is traditionally searched for in the difference of invariant masses $\Delta M = M_{K\pi\pi_{slow}} - M_{K\pi}$. Here the resolution is dominated by the measurement of the slow pion.

Fig. 1b) shows the mass difference ΔM for (K,π) combinations close to the D^0 mass ($|M_{K\pi} - M_{D^0}| < 80$ MeV/c^2). At the expected value $\Delta M \approx 145.4$ MeV/c^2 a clear signal for D^* production is observed. Fig. 1c) shows the mass spectrum of the (K,π) combinations, which give together with a third pion a D^* candidate ($|(M_{K\pi\pi_{slow}} - M_{K\pi}) - 145.4$ MeV/$c^2| < 1.5$ MeV/c^2). Here a clear signal of D^0 mesons is seen. The D^* (and the D^0) yield in the data is found to be compatible with the prediction by the RAPGAP model (unshaded histogram) using the parton densities obtained.

4 Conclusions

Two measurements of properties of the hadronic final state (energy flow and D^* meson production) in diffractive deep-inelastic scattering have been presented which are sensitive to contributions from a gluonic component in the diffractive exchange. The data were found to be described by a model for deep-inelastic $e\mathbb{P}$ scattering when using parton densities obtained from a DGLAP QCD analysis of $F_2^{D(3)}$ which have a dominant "leading" gluon component.

References

1. P.R. Newman, , *Inclusive measurements of diffraction in DIS and photoproduction*, this report.
2. H. Jung, Comp. Phys. Comm. 86 (1995), 147.
3. G. Ingelman and P.E. Schlein, Phys. Lett. B 152 (1985) 256.
4. G. Ingelman, *LEPTO Version 6.1* Proc. of the Workshop on Physics at HERA, Hamburg 1991, eds. W. Buchmüller and G. Ingelman, vol. 3, p. 1366.
5. B. Andersson, G. Gustafson and L. Lönnblad, Nucl. Phys. B339 (1990), 393.

JETS IN DIFFRACTIVE ep INTERACTIONS

J. THEISSEN
III. Physikalisches Institut B, Physikzentrum, RWTH Aachen,
D-52056 Aachen, Germany

Measurements of differential ep cross sections for 2 jet events in diffractive deep inelastic scattering and photoproduction with the H1 detector at HERA are presented. They are compared with predictions based on a partonic interpretation of the pomeron.

1 Introduction

The large rapidity gap events in ep collisions at HERA are attributed mostly to diffractive processes. The presence of jets in the final state indicates a hard pQCD subprocess. Therefore an analysis of 2 jet events can give insight into any partonic component of diffractive dynamics.

2 Data selection

The following study is based on e^+p data taken by H1 in 1994, corresponding to an integrated luminosity of $\mathcal{L}_{\rm int} = (2.25 \pm 0.045)\mathrm{pb}^{-1}$. To select deep inelastic scattering (DIS) events the scattered positron must be identified in the backward electromagnetic calorimeter with an energy of $E'_{e+} > 10\,\mathrm{GeV}$. The kinematical domain is further restricted to $0.05 < y < 0.6$ and $7.5\,\mathrm{GeV}^2 < Q^2 < 80\,\mathrm{GeV}^2$. Photoproduction events are selected using the H1 small angle electron tagger, which restricts the kinematical region to $0.25 < y < 0.7$ and $10^{-8}\,\mathrm{GeV}^2 < Q^2 < 0.01\,\mathrm{GeV}^2$. Subsamples of diffractive events are selected by demanding no signal above noise in the H1 forward detectors sensitive to particle production in the region $3.0 < \eta < 7.5$. The use of the forward detectors gives good acceptance in the kinematical region of high $E_{\rm t}$ jet production while keeping the background at an acceptable level (Fig. 1).

3 Cross sections for 2 jet production

The Monte Carlo generators RAPGAP (for DIS) and POMPYT (for photoproduction) were used to model diffractive hard scattering events for acceptance corrections. These models assume factorisation of the diffractive cross section into a pomeron flux and a photon pomeron cross section parameterised in terms of parton densities in the pomeron. For RAPGAP these were obtained from

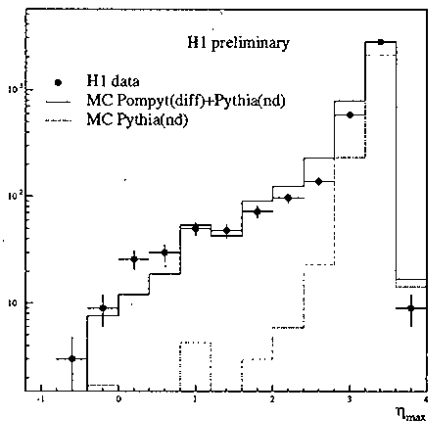

Figure 1: Distribution of $\eta_{\max}$, the maximum pseudorapidity of a calorimeter cluster with $E > 400$MeV, for 2 jet events in photoproduction. The solid line shows a combination of POMPYT and (non-diffractive) PYTHIA distributions normalised to the data. The dotted line shows the non-diffractive PYTHIA contribution.

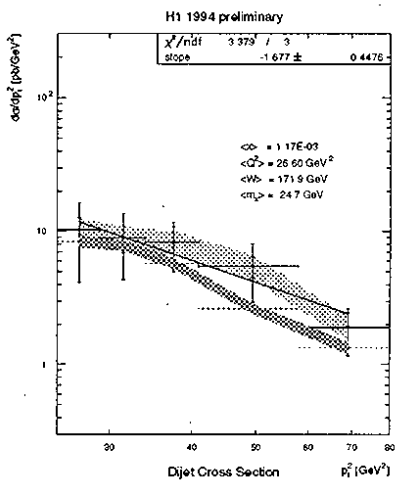

Figure 2: Differential ep cross section $d\sigma/dp^2_{t,\mathrm{jet}}$ for 2 jet events in diffractive DIS. The upper band indicates the common error due to the uncertainty of the energy scale in the main calorimeter. The lower band shows the RAPGAP prediction with its statistical error. The line represents a fit of the form $d\sigma/dp^2_{t,\mathrm{jet}} \propto p^{2n}_{t,\mathrm{jet}}$ with $n = -1.7$.

a QCD fit assuming DGLAP evolution in the $F_2^{D(3)}$ diffractive structure function (P. Newman, this report). For POMPYT three different parton densities were used: a hard gluon or hard quark density $\propto z(1-z)$ and a soft gluon density $\propto (1-z)^5$. The jet analysis in DIS and photoproduction was done with a CONE type algorithm using a combination of clusters and tracks as input. The DIS jet analysis uses a $25\times25\,(\eta,\phi)$ grid in the photon-pomeron rest frame with $-2.5 < \eta < 2.5$, a cone radius of $\Delta R = 1$ and $E_{t,\mathrm{jet}} \geq 5$ GeV. In total 95 events with 2 jets were found. The differential cross section $d\sigma/dp^2_{t,\mathrm{jet}}$ for inclusive 2 jet production corrected to the hadron level for $x_{\mathrm{IP}} < 0.1$ is shown in figure 2. The photoproduction jet analysis uses a $24 \times 24\,(\eta,\phi)$ grid in the lab frame with $-2.5 < \eta < 3.5$, a cone radius of $\Delta R = 1$ and $E_{t,\mathrm{jet}} \geq 5$ GeV. After a final jet cut of $-1.5 < \eta_{\mathrm{jet}} < 2.5$, a total of 441 events with 2 jets remained. The differential cross sections for inclusive 2 jet production corrected to the hadron level for $x_{\mathrm{IP}} < 0.05$ are shown in figure 3 ($d\sigma/dE_{t,\mathrm{jet}}$) and figure 4 ($d\sigma/d\eta_{\mathrm{jet}}$). In all plots the inner and outer error bars represent respectively the statistical error and the statistical and systematic error added in quadrature. The main contribution to the systematic errors comes from

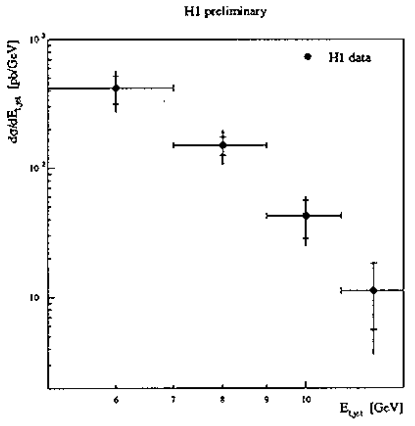

Figure 3: Differential ep cross section $d\sigma/dE_{t,\mathrm{jet}}$ for 2 jet events in diffractive photoproduction.

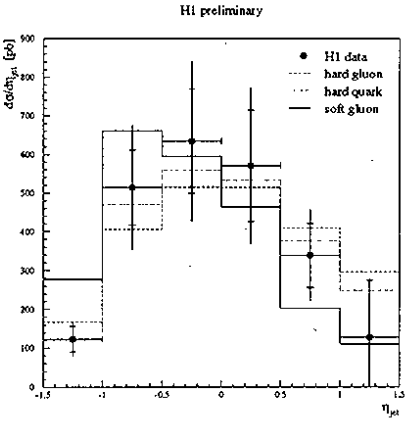

Figure 4: Differential ep cross section $d\sigma/d\eta_{jet}$ for 2 jet events in diffractive photoproduction. For comparison POMPYT predictions normalised to the data are also shown.

a 5% uncertainty in the energy scale of the main calorimeter. Other sources of systematic error considered are the uncertainty in the background subtraction, the acceptance correction, the luminosity measurement and the trigger efficiency.

4 Conclusions

Using the H1 forward detectors, samples of 2 jet events with a large rapidity gap were collected in DIS and photoproduction, which is strong evidence for hard subprocesses. The measured cross sections were corrected to the hadron level. In photoproduction there is no discrimination in the η_{jet} spectrum in shape to different POMPYT inputs. A prediction for the 2 jet cross section in DIS with the Monte Carlo generator RAPGAP using parton densities obtained from a QCD fit of $F_2^{D(3)}$ is close to the data.

Acknowledgments

I would like to thank Peter Uelkes for providing me with his results on diffractive DIS, Bertrand Laforge for checking them independendly and the DFG for financial support by a grant in the Graduiertenkolleg.

THRUST JET ANALYSIS OF DIFFRACTIVE DEEP-INELASTIC SCATTERING EVENTS

A.VALKÁROVÁ
Nuclear Center of Charles University, V Holešovičkách 2,Prague
Czech Republic

An analysis of thrust in the hadronic final state X of deep-inelastic diffractive electron-proton interactions is presented. The data were recorded by the H1 detector at HERA in 1994. A basic 2-jet structure is observed for which the values of thrust are smaller than those measured in e^+e^-annihilation, indicating that for a system of the same mass higher order perturbative QCD contributions are more important in this reaction than in e^+e^-annihilation. The P_t^2 distributions of thrust jets show alignment with the γ^*p collision axis, a large high P_t tail and an approximate independence of the hadron final state mass M_X.

We present results from a thrust analysis of hadronic final states in large rapidity gap (LRG) events emerging from the interaction of virtual photons with protons in ep collisions at the HERA collider

$$e + p \rightarrow e' + X + Y.$$

The systems X and Y are distinguished as those separated by the largest rapidity gap in the total hadronic final state. A total of 7132 such events, with an identified electron, corresponding to an integrated luminosity of $1.96pb^{-1}$ were selected with the H1 detector in 1994.
An estimate of non-diffractive contributions was subtracted with the help of the Monte Carlo model DJANGO for deep-inelastic events. The amount of non-diffractive background is small, and the results do not depend significantly on the background subtraction. For the thrust analysis we used events with mass M_X, $5 < M_X < 28.3\,\mathrm{GeV/c^2}$, $< Q^2 >= 22\,\mathrm{GeV}^2$ and scaled longitudinal momentum transfer from the proton $10^{-4} < x_{I\!P} < 0.05$, with $< x_{I\!P} >= 0.013$.

The thrust T is defined as

$$T = 1/M_X \cdot \max \sum_{i=1}^{N} |\vec{p}_i.\vec{n}|$$

with $\vec{p}_i$ the momentum of final state particle i and N the total number of particles. In the CMS of the X system $\sum_{i=1}^{N} \vec{p}_i = 0$, and the axis $\vec{n}$ is such that the energy flow projected into it is maximal. The orientation $\vec{n}$ and the event

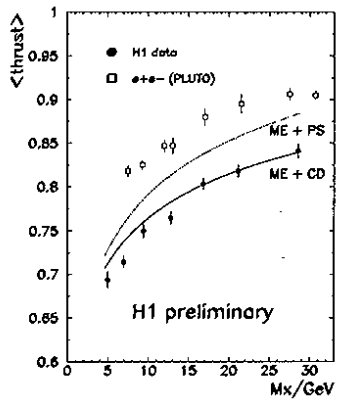

Figure 1: Average values of the thrust T, as a function of the hadronic mass M_X. Full circles: H1 data (fully corrected), open squares: e^+e^-annihilation (PLUTO). The lines are predictions of two versions of the RAPGAP matrix element simulation.

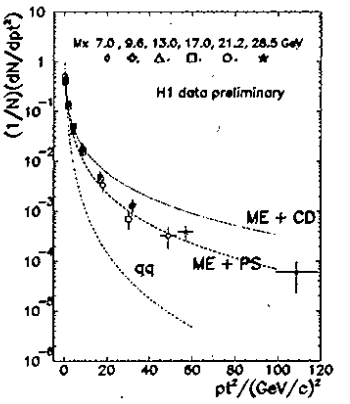

Figure 2: P_t^2 distributions of thrust jets for all M_X, the data points being shown at $< P_t^2 >$ of each P_t^2 interval, each of the distributions being normalized to 1. The curves are RAPGAP predictions for $24 < M_X < 36$ GeV/c^2, the one labeled qq is intended to modelise an aligned jet configuration.

shape given by T $(0.5 < T < 1)$ are obtained for each event. The variable P_t is defined as the thrust jet momentum transverse to the proton beam direction, as seen in the rest frame of the hadronic system X.

In the selected sample, the average thrust values are larger than 2/3 and are growing with M_X, which indicates a 2-jet pattern as the salient topological feature of the hadronic final state (see Fig. 1). The average thrust is smaller for the H1 deep-inelastic diffractive data than for e^+e^-annihilation, indicating that in diffractive dissociation configurations with higher parton multiplicities than in $e^+e^-$are created. Fig. 2 shows the P_t^2 distributions for all mass intervals. We observe a dominant alignment of the final state with the initial $\gamma^* p$ collision direction. However there is also a substantial P_t^2 tail for thrust jets up to 120 $(GeV/c)^2$ and a large fraction of events has $p_t^2 > 3\ GeV^2$ $(\sim 30\%)$. P_t^2 distributions follow an universal shape $1/\sigma \cdot \mathrm{d}\sigma/\mathrm{d}P_t^2(M_X, P_t^2) = A(M_X) \cdot G(P_t^2)$ for all mass intervals. These observations may be interpreted in terms of a significant contribution to deep-inelastic diffractive dissociation from photon-gluon fusion (as included for example in RAPGAP models).

PHOTOPRODUCTION OF VECTOR MESONS

S. SCHIEK, G. SCHMIDT

University of Hamburg, II. Institut für Experimentalphysik,
Notkestraße 85, 22607 Hamburg, Germany

Results obtained for photoproduction of vector mesons in γp interactions using the H1 detector at HERA are presented. The γp cross section for elastic ρ^0 production is found to be consistent with predictions from the soft pomeron model. J/ψ production is observed to increase strongly with the center of mass energy. This increase can be described in a QCD based model suggested by Ryskin using the gluon parametrisation MRS(A'). For inelastic J/ψ production the cross section is compared to NLO QCD calculations in a colour singlet model and agreement is found.

1 Introduction

At HERA 820 GeV protons collide with 27.5 GeV positrons. The resulting center of mass energy of $\sqrt{s} \approx 300$ GeV gives the possibility of studying the production of vector mesons (VM) in new kinematical regions. Here we review the photoproduction of vector mesons ($Q^2 \approx 0$).
The diffractive (elastic and proton dissociative) production of light vector mesons can be described within the Donnachie-Landshoff model (DL) [1]. This model is based on Regge phenomenology where the VM production is mediated by pomeron exchange. The cross section as a function of the photon proton center of mass energy $W_{\gamma p}$ is predicted to increase $\propto W_{\gamma p}^{0.32}$. The differential cross section $d\sigma/dt$, with t the momentum transfer squared at the proton vertex, is expected to be $\propto e^{bt}$.
An alternative model suggested by Ryskin et al. [2] describes the interaction between proton and heavy VM by the exchange of a gluon ladder which is calculable in perturbative QCD. The cross section is predicted to be proportional to the square of the gluon density in the proton.
The main inelastic J/ψ production process is the photon gluon fusion mechanism, which can be calculated in the colour singlet model. A gluon from the proton interacts with the photon emitted by the positron. The process is sensitive to the gluon density in the proton. For this reaction NLO QCD predictions have become available recently [3].

2 Experimental Setup

A detailed description of the H1 detector has been given elsewhere [4]. Elastic ρ^0-production is analysed in its dominant decay-channel $\rho^0 \to \pi^+\pi^-$ requiring exactly two tracks in the central tracking system.
J/ψ mesons are detected via their leptonic decays by demanding two identified electrons or muons in the H1 detector.
Elastic VM production is separated from proton dissociation processes using the signals in the forward detectors close to the proton beam:

- Forward part of the Liquid Argon calorimeter
- Forward Muon System
- Proton Remnant Tagger (placed $24\,m$ from the interaction point in the proton direction)

If there is any positive signal above noise in any detector the event is classified as due to proton dissociation, otherwise it is assumed to be elastic.

3 Diffractive vector meson production

The elastic cross section for ρ^0 meson production as a function of $W_{\gamma p}$ is shown in figure 1 (left). The H1 [5] and ZEUS measurements are consistent with the slight increase expected in the DL model.

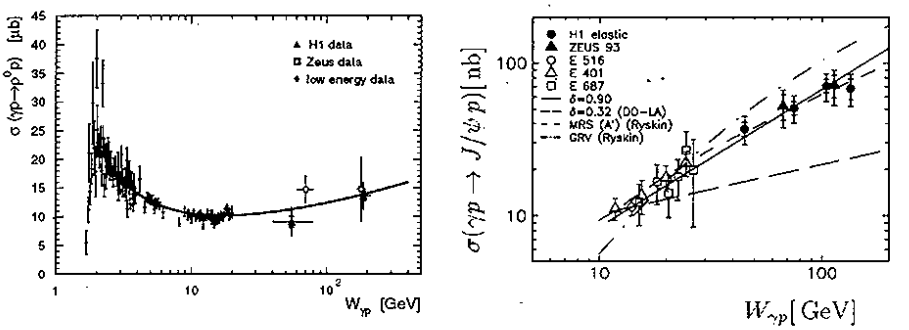

Figure 1: Total cross section for elastic ρ^0-production (left) and for elastic J/ψ-production (right). The inner error bars of the HERA points are statistical, the outer ones contain statistical and systematic errors added in quadrature.

An exponential fit of the t distribution yields a value for the slope parameter for elastic ρ^0 production of $b = (10.9 \pm 2.4 \pm 1.1)\,\mathrm{GeV}^{-2}$.

The elastic cross section for J/ψ meson production as a function of $W_{\gamma p}$ is shown in figure 1 (right)[6]. The prediction in the Donnachie-Landshoff model (long dashed line) cannot describe the HERA data. A better description is given by the pQCD calculations of the Ryskin model using the gluon parametrisation MRS(A') (short dashed line). A fit of the form W^δ to the H1 data yields a value of $\delta = 0.64 \pm 0.13$.
The cross section for proton dissociative J/ψ events is shown in figure 2 (left). A fit of the form W^δ gives the result $\delta = 1.2 \pm 0.2$.

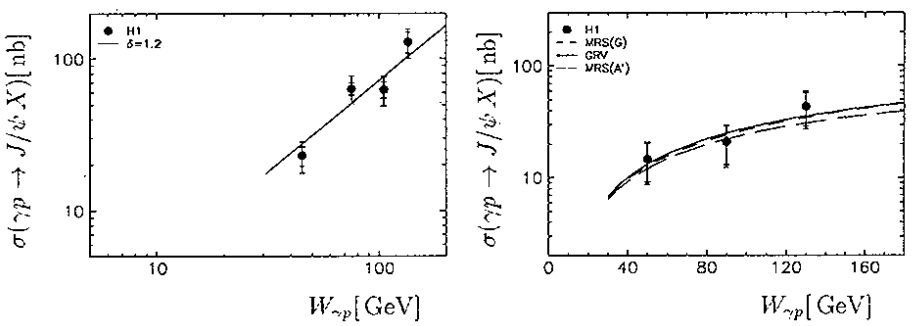

Figure 2: Total cross section for **proton dissociative** J/ψ-production (left) and for **inelastic** J/ψ-production in the range $z < 0.8$, $p_t^2 > 1\,GeV^2$ (right).

The result fitting the p_t^2 distribution for elastic J/ψ production ($t \approx -p_t^2$) is $b = (4.0 \pm 0.2 \pm 0.2)\,\mathrm{GeV}^{-2}$ (fig. 3 left) and $b = (1.6 \pm 0.3 \pm 0.1)\,\mathrm{GeV}^{-2}$ for J/ψ production with dissociation of the proton.
Diffractive production of ρ^0 and J/ψ mesons are consistent with s-channel helicity conservation.

4 Inelastic J/ψ production

The inelasticity z of the J/ψ meson is defined in the following way:

$$z = \frac{P_p \cdot P_\psi}{P_p \cdot q} \tag{1}$$

where P_p, P_ψ and (q) are the four vectors of the proton, the J/ψ meson and the photon. Elastic J/ψ events are produced at $z = 1$, whereas for inelastic production, z is below 1.
The cross section for inelastic events in a kinematical range with $z < 0.8$ and transverse momentum p_t^2 of the J/ψ meson above $1\,\mathrm{GeV}^2$ as function of $W_{\gamma p}$ is

shown in fig. 2 (right)[6]. The data points are compared to NLO QCD calculations[3] using a charm mass of $m_c = 1.4\,\mathrm{GeV}$ and $\Lambda_{\overline{MS}} = 300\,\mathrm{MeV}$. Agreement in shape and absolute normalisation between data and QCD predictions is found.
An exponential fit of the form $e^{-bp_t^2}$ to the differential cross section $d\sigma/dp_t^2$ yields a value for b of: $b = (0.39 \pm 0.06 \pm 0.03)\,\mathrm{GeV}^{-2}$, which agrees within errors with the NLO QCD prediction of $b = 0.3\,\mathrm{GeV}^{-2}$.

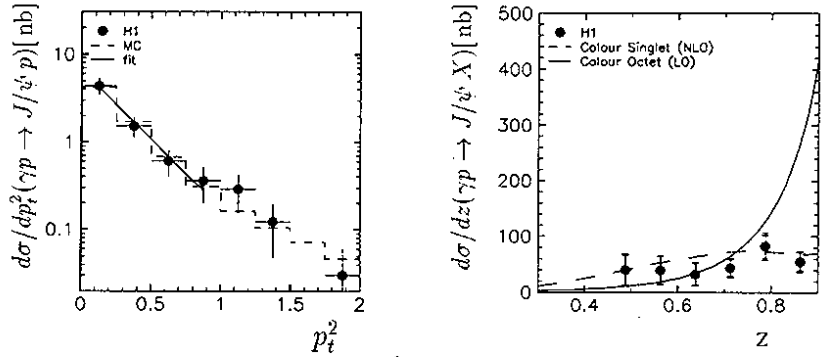

Figure 3: Differential cross section $d\sigma/dp_t^2$ for **elastic** J/ψ-production (left) and $d\sigma/dz$ for **inelastic** J/ψ-production in the range $p_t^2 > 1\,GeV^2$ (right).

The differential cross section $d\sigma/dz$ is well described by QCD calculations in colour singlet model (fig. 3 right). There is no evidence for the large colour octet contributions in the region $z > 0.75$, which are calculated[7] using colour octet matrix elements fitted to high energy $p\overline{p}$ data (Tevatron).

References

1. A. Donnachie and P.V. Landshoff, *Phys. Lett.* B348 (1995) 213; ibid. B296 (1992) 227.
2. M.G. Ryskin, R.G. Roberts. A.D. Martin and E.M. Levin, preprint DTP/95/96 CBPF-NF-079/95 RAL-TR-95-065 hep-ph/9511228 (1995), rev. February 1996.
3. M. Krämer, *Nucl. Phys.* **B459** (1996) 3.
4. I. Abt et al., H1 Coll., preprint DESY 96-001 (1996).
5. S. Aid et al., H1 Coll., *Nucl. Phys.* **B463** (1996) 3.
6. S. Aid et al., H1 Coll., preprint DESY 96-037 (1996)
7. M. Cacciari and M. Krämer, preprint DESY 96-005 (1996)

VECTOR MESON PRODUCTION AT HIGH Q^2

B. CLERBAUX
Université Libre de Bruxelles, Bd du Triomphe, 1050 Brussels, Belgium

Recent results for vector meson production at high Q^2 are reviewed. The total cross section for elastic electroproduction of ϱ, ϕ and J/ψ mesons for $Q^2 > 8$ GeV^2 and $<W> \approx 100$ GeV are measured at HERA with the H1 detector. The dependences of the photon-proton cross sections on Q^2, W and t are presented. The ϕ:ϱ and J/ψ:ϱ cross section ratios are determined. The elastic over dissociative ϱ cross section ratio is measured. Signals for ω and ϱ' production are presented.

We present results for electroproduction of vector mesons at large Q^2 ($Q^2 > 8$ GeV^2) and high $\gamma^{(*)}p$ centre of mass energy ($W \simeq 100$ GeV), for the reaction

$$e^{\pm}\, p \rightarrow e^{\pm}\, p\, V, \qquad V = \varrho, \omega, \phi, \varrho', J/\psi. \tag{1}$$

Results on ϱ and J/ψ mesons are published[1] (and are preliminary for the other vector mesons). Interactions where the proton diffractively dissociates are also studied for ϱ meson production (preliminary results). The analyses are based on an integrated luminosity of ≈ 3 pb^{-1} accumulated by H1 in 1994, the colliding particles being 27.5 GeV positrons or electrons and 820 GeV protons. These results are expected to shed light on the nature of the pomeron, either in a soft or a perturbative QCD approach, the latter being justified by the existence of a hard scale (high photon virtuality or high mass of the vector meson) (see ref. in [1]).
The cross section for elastic electroproduction of vector meson V is converted into the $\gamma^* p$ cross section using the flux of transverse virtual photons[1]. In the following all cross sections refer to the $\gamma^* p$ cross section. The kinematical variables are Q^2, W and the 4-momentum transfer squared to the proton: t. The cross section is parameterised according to a Regge approach and the optical theorem as: $d\sigma/dt \approx W^{4\varepsilon}.e^{bt}$, the Q^2 dependence being $d\sigma/dQ^2 \approx Q^{-2n}$ (or $(Q^2 + m^2_{J/\psi})^{-n}$ in case of the J/ψ production).

• W **dependence:** the W dependence of the elastic cross section for ϱ, ϕ and J/ψ meson production is shown in Fig. 1b, 1c and 1a respectively. For ϱ production, an increase faster than in photoproduction of the cross section with energy (from the NMC to H1 experiments) is observed at high Q^2. For the longitudinal cross section only, and after subtraction of the contribution of reggeon exchange, $\varepsilon = 0.18 \pm 0.05$ for Q^2=10 GeV^2, $\varepsilon = 0.14 \pm 0.06$

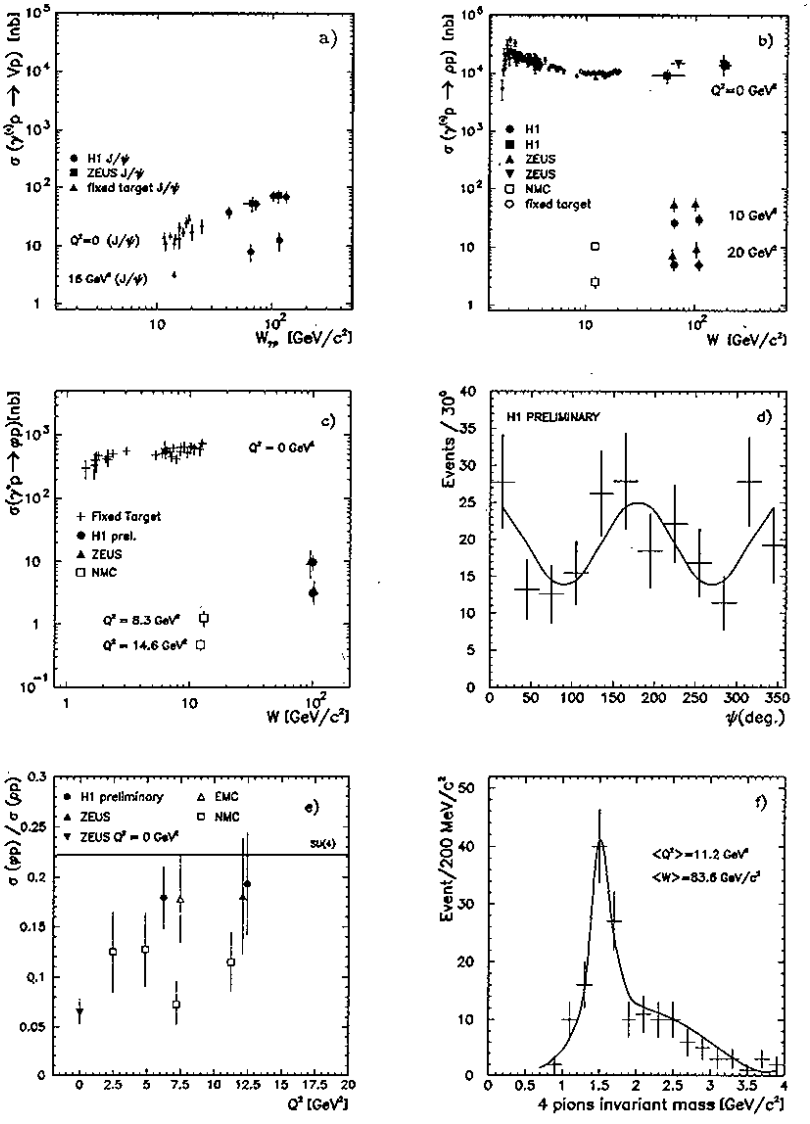

Figure 1: W dependence of the total $\gamma^* p$ cross section for the a) J/ψ, b) ϱ and c) ϕ meson; d) ψ angle distribution for elastic ϱ production; e) ϕ to ϱ elastic cross section ratio in function of Q^2; f) signal for ϱ' production (4π invariant mass distribution).

for Q^2=20 GeV^2. These results suggest that we are in a transition regime between soft ($\varepsilon = 0.08$) and hard physics processes [1]. For ϕ production, a stronger W dependence is found at high Q^2 (from NMC to H1 experiments) than in photoproduction. For J/ψ production, a steep increase of the cross section is observed with W both in photoproduction and at high Q^2, indicating that the hard regime is probably already reached at low Q^2 due to the mass of the charm quark.

• **t dependence:** the b slope parameters for the different vector mesons are listed in Tables 1 and 2. In comparison to elastic ϱ production, the slope is flatter for dissociative ϱ production (there is no proton form factor) and for J/ψ production (more compact meson wave function). Similarly to photoproduction, an indication for shrinkage of the elastic peak is observed at high Q^2, for elastic ϱ production, from the NMC to the HERA energies. Subtracting the non–resonant pion background with a similar procedure for the NMC and H1 data, the slope of the effective pomeron Regge trajectory, α', is found to be 0.28 $\pm$ 0.12 GeV^{-2} (for hadronic interactions, $\alpha' = 0.25$ GeV^{-2}).

• Q^2 **dependence:** the n parameters for the different vector mesons, presented in Table 1, are in general agreement with the models [1].

• **Angular decay distributions:** the probability r^{04}_{00} for a vector meson to be longitudinally polarised can be extracted from the distribution of $\cos\theta^*$ (θ^* is the angle, in the vector meson rest frame, between the direction of the positively charged decay particule and the the $\gamma^* p$ centre of mass system (helicity frame)). The ϱ and the ϕ mesons are mostly longitudinally polarised (Table 1), as predicted by most models. Assuming s–channel helicity conservation (SCHC), the density matrix element r^1_{1-1} can be computed from r^{04}_{00}. Yet, r^1_{1-1} can also be extracted from the ψ distribution (Fig. 1d) (ψ is the angle between the V decay plane and the scattered electron plane, in the $\gamma^* p$ cms). For elastic ϱ production, the equality within errors of the two values obtained for r^1_{1-1} (0.13 $\pm$ 0.03 and 0.14 $\pm$ 0.05 respectively) supports the SCHC hypothesis.

• **Total cross-section ratios:** the ratio of the dissociative over elastic ϱ cross sections is 0.59 $\pm$ 0.12 $\pm$ 0.12. No significant Q^2 ($Q^2 \in [8-36]$ GeV^2) and W ($W \in [60-180]$ GeV) dependence is observed. This ratio was also measured for J/ψ photoproduction [2]. These measurements allow the study of the factorisation of the diffractive cross section into two factors, describing respectively the processes at the photon and at the proton vertices. Factorisation would be manifest by the independence, with respect to the nature of

the produced vector meson, of the ratio of the elastic to proton dissociation cross sections, for t = 0. Taking into account the measured slopes, this ratio is 0.18 $\pm$ 0.09 for the ϱ and 0.43 $\pm$ 0.13 for the J/ψ. The ϕ:ϱ cross section ratio rises with Q^2 (Fig. 1e), and the rise is faster at high energy (HERA) than at lower energy (fixed target). The J/ψ:ϱ cross section ratio is very small in photoproduction (0.01 to 0.001), but is close to 1 at high Q^2 : 0.64 $\pm$ 0.13 ($Q^2 = 10$ GeV^2) and 1.3 $\pm$ 0.5 ($Q^2 = 10$ GeV^2) (Fig. 1a and 1b, same scale plots). This is consistent with a harder W dependence of the cross section for ϕ and for J/ψ than for ϱ mesons, and is compatible with the perturbative approach, based on the fact that the ϕ and J/ψ mesons have smaller spatial extent than the ϱ.

• **Other resonances:** signals for electroproduction of ω and ϱ' ($\varrho' \rightarrow 4\pi$) at large Q^2 are observed, the ϱ' meson decaying dominantly into a ϱ meson and a non resonant pion pair.

References

1. S. Aid et al., H1 Coll., *Nucl. Phys.* **B463** (1996) 3.
2. *Elastic and Inelastic Photoproduction of J/ψ Mesons at HERA*, preprint DESY 96-037. To be publ. in *Nucl. Phys.* **B**.

	b (GeV^{-2})	n	$<r_{00}^{04}>$
ϱ_{el}	$7.0 \pm 0.8 \pm 0.6$	$2.5 \pm 0.5 \pm 0.2$	$0.73 \pm 0.05 \pm 0.02$
ϱ_{diss}	$2.1 \pm 0.7 \pm 0.4$	$2.8 \pm 0.6 \pm 0.3$	$0.78 \pm 0.10 \pm 0.05$
ϕ	-	$2.0 \pm 0.6 \pm 0.1$	$0.77 \pm 0.11 \pm 0.02$
J/ψ	$3.8 \pm 1.2 \pm 1.8$	1.9 ± 0.3	-

Table 1: b slope (t distribution), n parameter (Q^2 distribution), and r_{00}^{04} parameter ($\cos\theta^*$ distribution), for different vector meson production. The ϱ dissociative and the ϕ results are still preliminary.

$40 < W < 140$ GeV/c^2	
$8 < Q^2 < 12$ GeV^2	$12 < Q^2 < 50$ GeV^2
$b = 7.8 \pm 1.0 \pm 0.7$ GeV^{-2}	$b = 5.7 \pm 1.3 \pm 0.7$ GeV^{-2}
$8 < Q^2 < 50$ GeV^2	
$40 < W < 80$ GeV/c^2	$80 < W < 140$ GeV/c^2
$b = 6.2 \pm 1.0 \pm 0.7$ GeV^{-2}	$b = 8.0 \pm 1.3 \pm 0.7$ GeV^{-2}

Table 2: Slopes of the t distributions for ϱ meson elastic production, for different Q^2 and W domains.